

MULTIVARIATE RATIONAL APPROXIMATION OF FUNCTIONS WITH CURVES OF SINGULARITIES*

NICOLAS BOULLÉ[†], ASTRID HERREMANS[‡], AND DAAN HUYBRECHS[‡]

Abstract. Functions with singularities are notoriously difficult to approximate with conventional approximation schemes. In computational applications they are often resolved with low-order piecewise polynomials, multilevel schemes or other types of grading strategies. Rational functions are an exception to this rule: for univariate functions with point singularities, such as branch points, rational approximations exist with root-exponential convergence in the rational degree. This is typically enabled by the clustering of poles near the singularity. Both the theory and computational practice of rational functions for function approximation have focused on the univariate case, with extensions to two dimensions via identification with the complex plane. Multivariate rational functions, i.e., quotients of polynomials of several variables, are relatively unexplored in comparison. Yet, apart from a steep increase in theoretical complexity, they also offer a wealth of opportunities. A first observation is that singularities of multivariate rational functions may be continuous curves of poles, rather than isolated ones. By generalizing the clustering of poles from points to curves, we explore constructions of multivariate rational approximations to functions with curves of singularities.

Key words. rational approximation, multivariate functions, singularity, least-squares

MSC codes. 41A20, 65E05, 32S70

1. Introduction. Rational approximations of functions provide a powerful representation of functions with singularities in comparison with polynomial approximation. Theoretical results pointing in this direction date back to Zolotarev [58] and Newman [43]. More recently, several algorithms for the numerical computation of rational approximations have been developed, which take advantage of these long known approximation results; these include the adaptive Antoulas–Anderson (AAA) algorithm [19, 34, 40, 41, 56], and the “lightning” method, which approximates solutions to differential equations on two-dimensional domains with corners using univariate rational functions [5, 10, 28, 29].

In one dimension one can employ a partial fraction representation with a polynomial part to represent a function f defined on an interval $I \subset \mathbb{R}$ as [32]:

$$(1.1) \quad f(z) \approx r(z) = \sum_{j=1}^{N_q} \frac{a_j}{z - q_j} + \sum_{j=0}^{N_p} b_j P_j(z).$$

This representation lies at the heart of the lightning method. Contrary to the AAA algorithm [40], which aims to solve the non-linear problem of best approximation by a rational function, the finite poles $\{q_j\}_{j=1}^{N_q}$ in (1.1) are fixed and selected a priori to cluster exponentially towards the singularities of the function f , of which the locations are assumed to be known. This results in a linear approximation problem, which achieves root-exponential convergence to functions with isolated singularities [24, 25,

*Submitted to the editors DATE.

Funding: N.B. was supported by an INI-Simons Postdoctoral Research Fellowship and the SciAI Center, funded by the Office of Naval Research (ONR) under Grant N00014-23-1-2729. A.H. is a PhD fellow of the Research Foundation Flanders (FWO), funded by grant 11P2T24N. D.H. was supported in part by FWO research project G088622N.

[†]Department of Applied Mathematics and Theoretical Physics, University of Cambridge, Cambridge, CB3 0WA, UK (nb690@cam.ac.uk).

[‡]Department of Computer Science, KU Leuven, 3001 Leuven, Belgium (astrid.herremans@kuleuven.be, daan.huybrechs@kuleuven.be).

26, 35], where the rate of convergence depends on the pole locations and the type of singularity [29, 53, 32]. Here, singularities are the points in the domain where the function either is discontinuous, e.g. $f(z) = \text{sign}(z)$, has a discontinuity in one of its derivatives, e.g. $f(z) = |z|$, or is non-differentiable, e.g. $f(z) = \sqrt{z}$. The addition of a smooth residual part consisting of polynomials $P_j(z)$ up to degree N_p in the rational approximation, as in (1.1), has been shown to improve the overall accuracy and numerical stability of the scheme [32]. Hence, [32] observed the convergence of (1.1) to functions x^α on $[0, 1]$ at optimal rates [47] by using least-square fitting. However, these approaches are usually limited to univariate rational expression and the approximation of functions with isolated singularities.

In this work, we are interested in computing multivariate rational approximations to functions with known curves of singularities. Inspired by the lightning approximation, we employ two-dimensional analogues of the partial fraction representation in (1.1) with clustering curves of poles. There are several applications motivating this study. First, the representation of curves of singularities is a major topic in image processing, leading to research on optimal sparse representations of piecewise smooth functions delineated by C^2 -curves achieved, e.g., by curvelets [11]. Second, the field of scientific machine learning aims to solve partial differential equations (PDEs) or learn solution operators associated with PDEs from data using a neural network representation [36]. These applications often involve the approximation of functions with shocks or discontinuities [37]. Recently, a neural network architecture based on rational activation functions, called rational neural networks [9], has been proposed to approximate Green's functions associated with linear PDEs [8]. When approximating Green's functions, rational neural networks, which are multivariate rational approximants, have poles that tend to cluster towards the diagonal of the domain, where Green's functions are singular [22]. The development of multivariate rational approximation algorithms to functions with curves of singularity should deepen our understanding of this phenomenon.

To the best of our knowledge, there have been limited explorations of computational techniques for multivariate rational approximation beyond [4, 7, 14, 15, 16, 57], and most of the previous studies in this topic only consider functions with isolated singularities. Theoretical convergence rates for multivariate rational approximations are derived in [18] by piecing together local polynomial approximations with rational partition-of-unity functions, extending the univariate ideas introduced by DeVore [17]. Then, the series of works by Cuyt and coauthors [14, 15, 16] constructs multivariate Padé approximations of the form $r(x, y) = P(x, y)/Q(x, y)$ to functions and show practical error bounds. More recently, [4] computes multivariate Padé approximations iteratively to discard potential spurious poles of the denominator $Q(x, y)$. However, this approach suffers when the function has singularities, and the determination of the polynomial degrees of the numerator and denominator is based on a heuristic method, which impacts the convergence rates.

A main result of this paper is a linear scheme to construct multivariate rational approximations to functions which are singular along the zero-levels of a multivariate polynomial. The scheme is based on well-chosen polynomial denominators associated with level curves of that same polynomial with complex shifts, in combination with exponential clustering of those shifts towards zero. Significant attention goes towards a numerically stable implementation of that scheme. We describe a series of examples with increasing level of complexity.

1.1. Organization of the paper. The paper is organized as follows. First, we introduce a multivariate rational approximation scheme for functions with singularities located along straight lines using a tensor-product representation in section 2. We prove robustness of the scheme with respect to the nature of the singularity. We then generalize this construction to functions with singularities along the diagonal of a domain using a piecewise rational approximation method in section 3. Finally, we consider the approximation of functions with algebraic curves of singularities in section 4 and conclude in section 5.

2. Tensor-product representation. We consider a tensor-product representation of a multivariate rational function to approximate two-dimensional functions $f(x, y)$ defined on the domain $\Omega = [0, 1]^2$ with singularities located along straight lines of the form $x = c$ or $y = c$, where $c \in [0, 1]$ is a constant. This construction is a generalization of (1.1) and consists of clustering lines of poles exponentially close to singularities.

2.1. Construction of the approximation. First, we consider the rational approximation of a function $f: (0, 1] \times [0, 1] \rightarrow \mathbb{R}$ with a singularity located at $x = 0$. We employ a basis of functions consisting of N_q finite poles, with associated partial fractions $\{\frac{q_j}{x-q_j}\}_{j=1}^{N_q}$, and a polynomial basis of degree N_p : $\{P_0, \dots, P_{N_p}\}$. Following [32, 54], we choose tapered exponentially clustered poles,

$$(2.1) \quad q_j = \pm i \exp(-\sigma(\sqrt{N_q} - \sqrt{j})), \quad 1 \leq j \leq N_q,$$

yet we cluster them along the imaginary axes (note the factor $\pm i$). This allows us to cluster poles exponentially close to singularities of the function inside the domain without introducing additional poles. The parameter $\sigma > 0$ in (2.1) controls the spacing between poles and is chosen to be $\sigma = 2\pi$ in this paper. This parameter choice is discussed later in subsection 2.5.

One can then approximate f by the tensor-product of a rational function in x with a polynomial in y as follows:

$$(2.2) \quad f(x, y) \approx r(x, y) = \sum_{j=1}^{N_q} \frac{q_j}{x - q_j} \sum_{k=0}^{N_p} a_{j,k} P_k(y) + \sum_{0 \leq j, k \leq N_p} b_{j,k} P_j(x) P_k(y).$$

We adopt the “lightning + polynomial approximation” scheme of [32], which consists of choosing the polynomial degree as $N_p = \mathcal{O}(\sqrt{N_q})$. While the convergence rate of a multivariate polynomial approximation is dictated by the Euclidean degree of the multivariate polynomial rather than the maximal degree [51], this representation allows for an efficient least-square solver exploiting the tensor-product structure of (2.2). To that end, the rational function r can be written as

$$r(x, y) = \begin{bmatrix} \frac{q_1}{x-q_1} & \cdots & \frac{q_{N_q}}{x-q_{N_q}} & P_0(x) & \cdots & P_{N_p}(x) \end{bmatrix} C \begin{bmatrix} P_0(y) \\ \vdots \\ P_{N_p}(y) \end{bmatrix},$$

where the matrix $C \in \mathbb{C}^{(N_q+N_p+1) \times (N_p+1)}$ contains the coefficients $\{a_{j,k}\}$, $\{b_{j,k}\}$ as

follows,

$$C = \begin{bmatrix} a_{1,0} & \cdots & a_{1,N_p} \\ \vdots & \ddots & \vdots \\ a_{N_q,0} & \cdots & a_{N_q,N_p} \\ b_{0,0} & \cdots & b_{0,N_p} \\ \vdots & \ddots & \vdots \\ b_{N_p,0} & \cdots & b_{N_p,N_p} \end{bmatrix}.$$

We then solve the following least-square system to find the coefficient matrix C :

$$(2.3) \quad \min_{C \in \mathbb{C}^{(N_q+N_p+1) \times (N_p+1)}} \|ACB^\top - F\|_{\mathbb{F}},$$

where $F \in \mathbb{C}^{M_x \times M_y}$, $A \in \mathbb{C}^{M_x \times (N_q+N_p+1)}$, and $B \in \mathbb{C}^{M_y \times (N_p+1)}$ are matrices containing function values of f at a set of sampling points $\{(x_i, y_j)\}_{i,j}$, function values of the basis functions in the x variable at $\{x_i\}_i$, and function values of the basis functions in the y variable at $\{y_j\}_j$, respectively.

The $M_x \times M_y$ sampling points are chosen to be a superposition of a product grid of $M_p \times M_p$ Chebyshev points in the x and y coordinates, and a product of M_q points clustering exponentially fast to $x = 0$ with M_p Chebyshev points in the y coordinates (see Figure 1(a)). Thus, $M_x = M_p + M_q$ and $M_y = 2M_p$. We typically choose a certain amount of oversampling,

$$M_q = 3N_q \quad \text{and} \quad M_p = 2N_p.$$

The clustering points $\{x_i\}_{i=1}^{M_q}$ are logarithmically spaced in order to resolve the singularity of the function f at $x = 0$, our practical implementation being

$$x_i = 10^{-16+16(i-1)/(M_q-1)}, \quad 1 \leq i \leq M_q.$$

The total number of sampling points is $M_x \times M_y = 2M_p^2 + 2M_pM_q$.

The tensor-product method described in this section generalizes naturally when the function has several straight-line singularities located at different points in the domain, including a mix of horizontal and vertical lines. As an example, for a function with singularities located at $x = x_0$ and $y = y_0$, the rational approximant has the form

$$(2.4) \quad r(x, y) = [R(x, x_0) \quad P(x)] C \begin{bmatrix} R(y, y_0)^\top \\ P(y)^\top \end{bmatrix},$$

where the term $R(z, z_0)$ contains the basis of rational functions whose poles cluster exponentially close to $z = z_0$ as $R(z, z_0) = \left[\frac{p_1}{(z-z_0)-q_1} \quad \cdots \quad \frac{p_N}{(z-z_0)-q_{N_1}} \right]$, and $P(z) = [P_0(z) \quad \cdots \quad P_{N_p}(z)]$. Here, C is a square matrix of $(N_q + N_p + 1) \times (N_q + N_p + 1)$ coefficients. Similar constructions can be made involving more terms $R(x, x_k)$ and $R(y, y_k)$ when more singularities are present. The sample grid is constructed as a superposition of Chebyshev points in the x and y coordinates, along with points clustering exponentially fast to each singularity (see Figure 1(a)).

A variant of this scheme when the function is periodic in one direction, such as functions defined on the unit disk, employs trigonometric polynomials in the rational representation (2.2), along with trigonometric (i.e., equispaced) sampled points. For example, Figure 1(b) displays the sample grid for a function defined on the unit

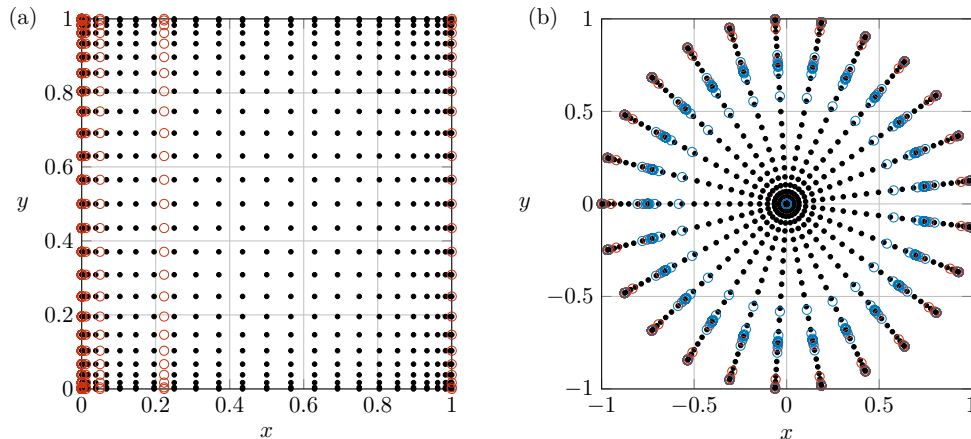


Fig. 1: (a) The product grid of sample points used for evaluating a function defined on a square domain. The sample grid is a superposition of product Chebyshev points in the x and y coordinates shown as black dots, and a product of points clustering exponentially fast to $x = 0$ with Chebyshev points in the y coordinates, highlighted in red. (b) Sample grid for a function defined on the unit disk with singularities located at $r = 3/4$ and $r = 1$. The grid is constructed using Chebyshev points in the radial direction and trigonometric points in the angular direction, along with points clustering towards $r = 3/4$ (in blue) and $r = 1$ (in red) in the radial direction.

disk with singularities located at $r = 3/4$ and $r = 1$. The grid is constructed using Chebyshev points in the radial direction and trigonometric points in the angular direction (as black dots), along with points clustering towards $r = 3/4$ (in blue) and $r = 1$ (in red) in the radial direction.

2.2. Regularized least squares fitting. In general, the system matrices A and B introduced in (2.3) are heavily ill-conditioned, yet accurate approximations can still be found using effective regularization techniques [1, 2, 32]. We regularize and solve (2.3) with the truncated singular value decomposition (SVD) algorithm [21, 31, 42]. Due to the tensor-product structure of the rational representation (2.2), the problem (2.3) is equivalent to the following linear least squares problem:

$$(2.5) \quad \min_{\mathbf{c} \in \mathbb{C}^{(N_q + N_p + 1)(N_p + 1)}} \|(B \otimes A)\mathbf{c} - \mathbf{f}\|_2,$$

where $\mathbf{c} = \text{vec}(C)$ and $\mathbf{f} = \text{vec}(F)$ are the vectors obtained by stacking the columns of C and F . The procedure described in Algorithm 2.1 solves this least squares problem using the truncated SVD of the matrix $B \otimes A$. Note that the algorithm employs B^\top rather than B^* even when B is complex-valued and that \odot denotes the Hadamard product of matrices.

We emphasize that Algorithm 2.1 is computationally efficient and exploits the tensor-product approximation of the rational representation (2.2) as it only requires to compute the singular value decomposition of the matrices A and B instead of the SVD of the large Kronecker product $B \otimes A$. When the rational or polynomial degree is large, one can alternatively reduce the computational cost by computing the truncated SVD of A and B using the randomized SVD [30, 39].

Algorithm 2.1 Truncated SVD solver

Input: $A \in \mathbb{C}^{M_A \times N_A}$, $B \in \mathbb{C}^{M_B \times N_B}$, $F \in \mathbb{C}^{M_A \times M_B}$, relative tolerance $\epsilon > 0$

Output: $C \in \mathbb{C}^{N_A \times N_B}$ such that $ACB^\top \approx F$

- 1: Compute the SVD of A and B , $A = U_A \Sigma_A V_A^*$ and $B = U_B \Sigma_B V_B^*$.
- 2: Compute $S = \text{diag}(\Sigma_A^\dagger)(\text{diag}(\Sigma_B^\dagger))^\top$.
- 3: Set all entries of S larger than $1/(\epsilon \sigma_1(A) \sigma_1(B))$ to zero.
- 4: Return $C = V_A(S \odot (U_A^* F (U_B^*)^\top)) V_B^\top$.

The ill-conditioning of the matrices A and B , and hence of $B \otimes A$, is a consequence of the (near-)redundancy of the proposed basis functions in (2.2). It indicates that the error on the coefficients can be arbitrarily large; however, this does not mean that a small residual cannot be obtained. We provide a bound on the residual in Theorem 2.1 by exploiting an existing result [12, Lem. 3.3] on the accuracy of regularized least squares fitting. The typical result in ill-conditioned least squares fitting is that solutions with small residual can be found numerically if such a solution exists with modest coefficient norm. In addition, a high level of oversampling ensures that a small residual corresponds to high approximation accuracy.

THEOREM 2.1. *Let $A \in \mathbb{C}^{M_A \times N_A}$, $B \in \mathbb{C}^{M_B \times N_B}$, $F \in \mathbb{C}^{M_A \times M_B}$, and choose a relative threshold parameter $0 < \epsilon < 1$. Let $C \in \mathbb{C}^{N_A \times N_B}$ be the coefficient matrix computed by Algorithm A.1. Then,*

$$\|F - ACB^\top\|_F \leq \inf_{X \in \mathbb{C}^{N_A \times N_B}} \{ \|F - AXB^\top\|_F + \epsilon \|A\|_2 \|B\|_2 \|X\|_F \}.$$

Proof. We first prove that Algorithm 2.1 solves (2.5), and hence (2.3), using the truncated SVD of $B \otimes A$. [55] shows that the singular value decomposition of $B \otimes A$ follows from the SVD of A and B as

$$B \otimes A = (U_B \otimes U_A)(\Sigma_B \otimes \Sigma_A)(V_B \otimes V_A)^*.$$

Consider now the diagonal matrix $\Sigma = \Sigma_B \otimes \Sigma_A$ containing the singular values of $B \otimes A$:

$$\{ \sigma_k(A) \sigma_l(B) \mid 1 \leq k \leq \min(M_A, N_A), 1 \leq l \leq \min(M_B, N_B) \}.$$

All singular values smaller than $\epsilon \sigma_1(A) \sigma_1(B)$ are set to zero in Algorithm 2.1, resulting in a new matrix denoted by Σ_ϵ . A coefficient vector \mathbf{c} can now be computed using the Moore–Penrose pseudoinverse, denoted by \dagger , of the truncated SVD of $B \otimes A$, resulting in

$$\mathbf{c} = (V_B \otimes V_A) \Sigma_\epsilon^\dagger (U_B \otimes U_A)^* \mathbf{f}.$$

This can again be condensed into a matrix equation using the dense matrix $S \in \mathbb{C}^{\min(M_A, N_B) \times \min(M_B, N_B)}$ whose entries contain $\text{diag}(\Sigma_\epsilon)$, i.e., the (truncated) singular values of $B \otimes A$. Also using the identities $(A \otimes B)^* = A^* \otimes B^*$ and $\text{vec}(AXB^\top) = (B \otimes A) \text{vec}(X)$ we obtain

$$C = V_A(S \odot (U_A^* F (U_B^*)^\top)) V_B^\top.$$

This proves that Algorithm 2.1 computes a solution to the least squares problem (2.5) using the truncated SVD of $B \otimes A$. A bound on the residual follows by applying [12, Lem. 3.3] with an absolute truncation threshold $\varepsilon = \epsilon \|A\|_2 \|B\|_2$,

$$\|\mathbf{f} - (B \otimes A) \mathbf{c}\|_2 \leq \inf_{\mathbf{x} \in \mathbb{C}^{N_A N_B}} \{ \|\mathbf{f} - (B \otimes A) \mathbf{x}\|_2 + \epsilon \|A\|_2 \|B\|_2 \|\mathbf{x}\|_2 \},$$

which is equivalent to

$$\|F - ACB^\top\|_{\mathbb{F}} \leq \inf_{X \in \mathbb{C}^{N_A \times N_B}} \{\|F - AXB^\top\|_{\mathbb{F}} + \epsilon \|A\|_2 \|B\|_2 \|X\|_{\mathbb{F}}\},$$

where we used the fact that $\|X\|_{\mathbb{F}} = \|\text{vec}(X)\|_2 = \|\mathbf{x}\|_2$. \square

Theorem 2.1 shows that the residual is of order ϵ for functions f that can be approximated to within ϵ by a tensor-product approximant with bounded coefficients, i.e., high accuracy is obtained if there exist coefficients $X \in \mathbb{C}^{N_A \times N_B}$ such that $\|F - AXB^\top\|_{\mathbb{F}} \approx \epsilon$ with $\|X\|_{\mathbb{F}} \approx 1$. Thus, the condition number of the system does not adversely affect the accuracy of the calculations. The numerical examples in this paper use $\epsilon = 10^{-14}$. This parameter choice is discussed later in subsection 2.5.

Remark 2.2. An alternative approach to solving the least squares problem is to regularize A and B independently, rather than the product $B \otimes A$. This results in a more straightforward algorithm, explained in Appendix A, with similar theoretical guarantees (see Theorem A.1). However, this approach is less numerically stable for very small truncation thresholds, leading to our preference for Algorithm 2.1.

2.3. Convergence analysis. In [29, §2], root-exponential convergence is proven for the lightning approximation to a univariate complex function on a polygonal subset of \mathbb{C} with branch point singularities at the corners. We prove a similar result for the proposed bivariate approximant for functions on a rectangular subset of \mathbb{R}^2 with a continuum of singularities along one edge. To that end, we formulate a few lemmas in Appendix B that summarize and slightly extend the results of [29]. The results imply robustness of rational approximation with clustering poles with respect to the order of the singularity. Based on those results, we can show the existence of bivariate rational approximations to functions with singularities along an edge of a rectangle, even if the order of the singularity varies along the edge.

THEOREM 2.3 (Multivariate rational convergence analysis). *Let Π be the square domain $(0, 1] \times [0, 1]$ and $f : \Pi \rightarrow \mathbb{C}$ be an analytic function in Π , with the following three properties near the left segment $\{0\} \times [0, 1]$:*

1. *The boundary trace defined as $h(z_2) = f(0, z_2)$ is an analytic function of $z_2 \in [0, 1]$.*
2. *For each $z_2 \in [0, 1]$, f satisfies the following uniform growth condition:*

$$f(z_1, z_2) - h(z_2) = \mathcal{O}(|z_1|^\delta), \quad \text{as } z_1 \rightarrow 0,$$

for some $\delta > 0$ that is independent of z_2 .

3. *For each $z_2 \in [0, 1]$, the univariate function $f(\cdot, z_2)$ can be analytically continued to a disk near $z_1 = 0$ with a slit along the negative real axis.*

Then, for $1 \leq n < \infty$, there exist a multivariate rational function r_n , of the form

$$(2.6) \quad r_n(z_1, z_2) = \sum_{j=0}^{n-1} \frac{s_j(z_2)}{z_1 - \beta_j} + p(z_1, z_2),$$

such that

$$\|f - r_n\|_{\infty, \Pi} = \mathcal{O}(e^{-C\sqrt{n}}), \quad \text{as } n \rightarrow \infty,$$

for some $C > 0$. Here, $s_j(z_2)$ is a univariate polynomial of degree scaling as $\mathcal{O}(\sqrt{n})$, $p(z_1, z_2)$ is a bivariate polynomial of degree scaling as $\mathcal{O}(\sqrt{n})$ as $n \rightarrow \infty$, and the poles β_j are finite and exponentially clustered towards 0, with arbitrary clustering parameter $\sigma > 0$ as defined by (B.1).

Proof. Since the function h is analytic on $[0, 1]$, and hence on a neighborhood in the complex z_2 -plane, it can be approximated with exponential convergence by polynomials. Its approximation can be incorporated into the polynomial term $p(z_1, z_2)$, and it remains to describe the approximation of the function $u : \Pi \rightarrow \mathbb{C}$ defined as

$$u(z_1, z_2) = f(z_1, z_2) - f(0, z_2) = f(z_1, z_2) - h(z_2), \quad (z_1, z_2) \in \Pi.$$

Let $z_1 \in (0, 1]$, then the Chebyshev projection of degree K to the function $u(z_1, \cdot)$, where the Chebyshev polynomials T_k are scaled to $[0, 1]$, is [52, Thm. 3.1]

$$\hat{u}(z_1, z_2) = \sum_{k=0}^K 'a_k(z_1)T_k(z_2), \quad a_k(z_1) = \frac{2}{\pi} \int_0^1 u(z_1, z_2) \frac{T_k(z_2)}{\sqrt{z_2 - z_2^2}} dz_2, \quad z_2 \in [0, 1],$$

where $'$ indicates that the first term in the series is halved. The functions $a_k : (0, 1] \rightarrow \mathbb{C}$ satisfy the conditions of Lemma B.2 and can therefore be approximated with root-exponential accuracy by a degree $(n + m, n)$ rational function \hat{a}_k as

$$\hat{a}_k(z_1) = \sum_{j=0}^{n-1} \frac{s_j^k}{z_1 - \beta_j} + p_k(z_1), \quad 0 \leq k \leq K, \quad z_1 \in (0, 1].$$

Here, the poles β_j defined by (B.1) are fixed, but the degree m polynomial p_k and the coefficients $s_j^k \in \mathbb{C}$ are dependent on k . Since D , b and Ω introduced in Lemma B.2 can be chosen such that they are independent of k , and also $\|a_k\|_{\infty, \Omega}$ can be bounded independently of k (since the Chebyshev polynomials themselves are uniformly bounded), the error of each term is bounded by

$$\|a_k - \hat{a}_k\|_{\infty, [0, 1]} \leq Ae^{-C\sqrt{n}},$$

for sufficiently large n and for some constants $A, C > 0$. The fact that $\|a_k\|_{\infty, \Omega}$ is bounded independently of k also implies that one can choose the same degree $m = E\sqrt{n}$ for each k for a fixed $E > 0$. Furthermore, we can choose the same K for each $z_1 \in (0, 1]$, based on the smallest Bernstein ellipse in which $u(z_1, \cdot)$ is analytic as a function of z_2 , such that

$$(2.7) \quad \|u - \hat{u}\|_{\infty, \Pi} = \mathcal{O}(e^{-C'K}),$$

for some $C' > 0$ depending on the radius of that ellipse.

Substituting $\hat{a}_k(z_1)$ into $\hat{u}(z_1, z_2)$ results in a bivariate rational function

$$(2.8) \quad q(z_1, z_2) := \sum_{k=0}^K ' \hat{a}_k(z_1)T_k(z_2) = \sum_{j=0}^{n-1} \frac{s_j(z_2)}{z_1 - \beta_j} + \sum_{k=0}^K p_k(z_1)T_k(z_2),$$

where $s_j := \sum_{k=0}^K s_j^k T_k$ is a polynomial of degree K for $0 \leq j \leq n - 1$. The approximation error between u and q can be bounded uniformly in Π using the triangular inequality as

$$\|u - q\|_{\infty, \Pi} \leq \|u - \hat{u}\|_{\infty, \Pi} + \|\hat{u} - q\|_{\infty, \Pi}.$$

The first term on the right-hand side is bounded by (2.7). Considering the second term and the definition of q in (2.8), for $(z_1, z_2) \in \Pi$ we have

$$|\hat{u}(z_1, z_2) - q(z_1, z_2)| \leq \sum_{k=0}^K |a_k(z_1) - \hat{a}_k(z_1)| |T_k(z_2)|,$$

which we bound by taking the supremum over $z_1 \in [0, 1]$ and $z_2 \in [0, 1]$ as

$$(2.9) \quad \|\hat{u} - q\|_{\infty, \Pi} \leq \sum_{k=0}^K \|a_k - \hat{a}_k\|_{\infty, [0,1]} \|T_k\|_{\infty, [0,1]} = \mathcal{O}(Ke^{-C\sqrt{n}}).$$

We now combine (2.7) and (2.9) and select $K = (C/C')\sqrt{n}$ such that

$$\|u - q\|_{\infty, \Pi} = \mathcal{O}\left(\sqrt{n}e^{-C\sqrt{n}}\right) = \mathcal{O}\left(e^{-C\sqrt{n}/2}\right),$$

which concludes the proof. \square

We make a few remarks about the scope of this result. First, note that the choice of poles used in Theorem 2.3 (defined by (B.1)) differs from the proposed poles in subsection 2.1 in multiple ways. The latter uses two sets of imaginary poles, allowing to approximate singularities in the interior of the domain, and uses a tapered distribution of the poles, which has been shown to increase the convergence rate for branch point singularities [53]. Also, a scaling $R = 1$ is used, which does not impact the convergence of the rational approximation in practice, as explained in Appendix B. More information on the choice of poles, including the spacing parameter σ , is given in subsection 2.5.

Second, although the basis of the approximation space has the structure of a tensor product, namely a rational function in z_1 times a polynomial in z_2 , the space itself captures more interesting functions than low-rank functions. In particular the space contains approximations to functions with continuously varying orders of algebraic singularities, as long as there is a lower bound $\delta > 0$ on the order.

Third, the result of this theorem is restricted to functions with singularities along one edge, but there is a straightforward generalization of the approximation space to deal with singularities along multiple edges. Indeed, the univariate rational approximations considered in [32] have the form of partial fractions in combination with a polynomial term, hence a tensor product in the x and y variables leads to four terms in total. This is exactly the form we propose in (2.4). The results of [32] immediately translate into favorable approximation results for separable functions such as $f(x, y) = \sqrt{x}\sqrt{y}$. However, due to the robustness of the clustering poles with respect to the nature of the singularity, the space can accurately capture a much broader class of functions. Particularly relevant classes of functions are solution sets of elliptic PDEs with analytic data, which give rise to edge and corner singularities, see [49, Sec. 1] and references therein. These function spaces have been extensively studied to investigate the convergence behavior of finite element methods with hp -refinement and neural networks, which are known to be related to rational approximation methods with exponentially clustered poles [35]. Recent research [38] proves exponential expressivity with stable ReLU neural networks for such classes on polytopal domains by constructing tensorized hp -approximations to point and edge singularities.

Finally, we note that the statement of the proof is about the accuracy of the approximation space, and not about the stability of the representation in partial fractions form. The latter is important in practice, and we will carefully select the normalization of the basis functions and rational and polynomial degrees such that the norms of the coefficients in the chosen basis are modest in size (see [1, 2] for the general theory and [32, §4] for a discussion in the context of rational approximations). We do not actually prove that such representations always exist. A result along those lines is proven for the specific case of rational approximations to \sqrt{z} in [32]. We emphasize

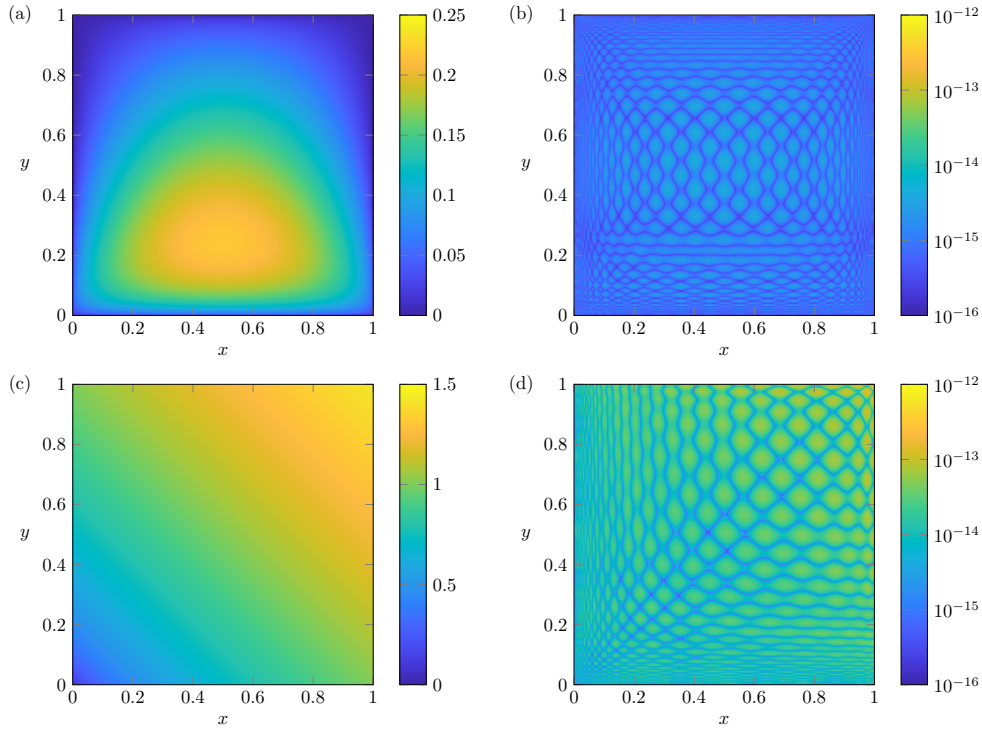


Fig. 2: (a) The function $f(x, y) = (x(1-x))^{\frac{1}{4}+y} \sqrt{y(1-y)}$ along with (b) the approximation error $|f(x, y) - r(x, y)|$ by a tensor-product rational function r with lines of poles clustering towards the boundary of the square. (c)-(d) Same as (a)-(b) with the function $f(x, y) = \sqrt{x+y}$ and its rational approximant with poles located near the lines $x = 0$ and $y = 0$.

that numerical stability of the representation and of the least squares approximation algorithm is the reason why approximations can be found to very high accuracy for the examples in this paper, in some cases even close to machine precision.

2.4. Numerical examples. As a first numerical example, we consider the approximation of the function $f(x, y) = (x(1-x))^{\frac{1}{4}+y} \sqrt{y(1-y)}$ on the unit square. This function has singularities on all four edges of the square, with varying order. We approximate f using a tensor-product rational function with poles clustering towards the boundary at $x = 0$, $x = 1$, $y = 0$, and $y = 1$, using the method introduced in subsection 2.1. Here, we use a rational degree of $N_q = 150$ along with a polynomial degree of $N_p = 16$ for the smooth part of the approximation. We display in Figure 2(a) the function f that we aim to approximate along with the approximation error $|f(x, y) - r(x, y)|$ by the rational function r in Figure 2(b). We evaluate the rational approximant on an equispaced grid with 1000×1000 points and obtain a maximum approximation error of 4.6×10^{-15} . Moreover, the residual of the least-square problem (2.3) has infinity norm equal to 1.5×10^{-14} , which is of the same order of magnitude as the approximation error, indicates that the error is uniformly small even exponentially close to the boundary.

Then, we examine the function $f(x, y) = \sqrt{x+y}$ defined on $[0, 1]^2$ with square-

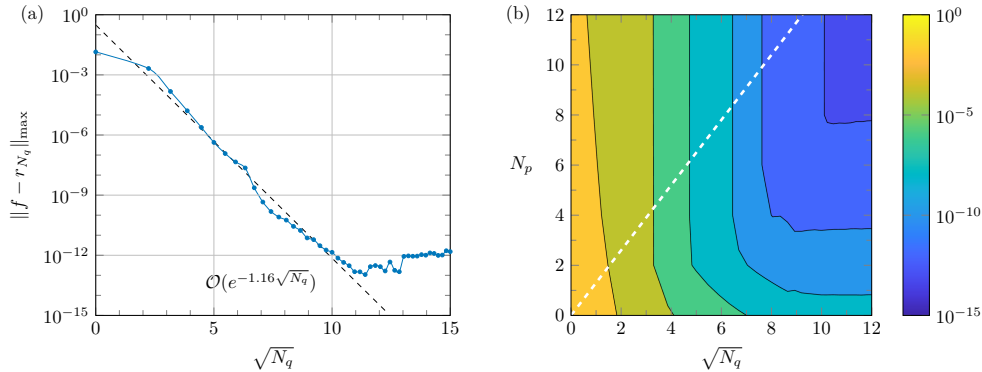


Fig. 3: (a) Convergence of the multivariate rational approximant r to the function $f(x, y) = \sqrt{x+y}$ with respect to the square-root of the rational degree N_q . The dashed line illustrates the empirical convergence rate. (b) Approximation error between f and its rational approximant as a function of the square-root of the rational degree N_q and the polynomial degree N_p . The white dashed line shows the scaling of the polynomial degree $N_p = 1.3\sqrt{N_q}$ employed in this work. Both figures display the maximum error on a fine independent grid, similarly distributed as the sampling grid.

root singularity at $(0, 0)$. We note that this function, plotted in Figure 2(c), is not separable as it cannot be written as a product of two one-dimensional functions. We visualize the approximation error with a rational function of degree $N_q = 150$ with lines of poles at $x = 0$ and $y = 0$, computed using the tensor-product method of subsection 2.1 in Figure 2(b). We observe that the approximation error is relatively uniform on the domain, with a maximum error of 1.6×10^{-13} on a 1000×1000 equispaced grid. In Figure 3(a), we plot the maximum approximation error of the rational function with respect to the square-root of the rational degree N_q on a grid consisting of points that are distributed similarly as the sampling points, therefore containing points clustered towards the singularity, yet which is much finer than the sampling grid. The maximum error on this grid gives a reliable indication of the uniform error on $[0, 1] \times [0, 1]$. Here, we fix $N_p = 16$ and $M_1 = M_2 = 1200$ to observe the decay rate of the error. We find that the approximation error decays at a square-root exponential rate, i.e.,

$$\|f - r_{N_q}\|_{\max} = \mathcal{O}(e^{-1.16\sqrt{N_q}}),$$

as illustrated by the dashed line in Figure 3(a), which is in agreement with the theoretical results of subsection 2.3. Next in Figure 3(b), we display the uniform approximation error between f and its rational approximant as a function of the rational and polynomial degrees N_q and N_p . We observe that the approximation error decays root-exponentially fast with respect to N_q for a sufficiently high polynomial degree N_p . The figure confirms that a polynomial degree scaling as $N_p = \mathcal{O}(\sqrt{N_q})$ is sufficient.

Finally, we consider the multivariate rational approximation of the following function defined on the unit disk $\Omega = D(0, 1)$:

$$(2.10) \quad f(r, \theta) = \begin{cases} \cos(10r + 10\theta), & r \in [0, 3/4], \theta \in [-\pi, \pi), \\ -\sqrt{1-r} \cos(10r - 10\theta), & r \in (3/4, 1], \theta \in [-\pi, \pi). \end{cases}$$

We note that this function has a square-root singularity along the unit circle and a discontinuity at $r = 3/4$. To approximate this function, we use a tensor-product rational function consisting of a mixed Chebyshev polynomial basis and rational functions in the radial direction r with poles clustering towards $r = 1$ and $r = 3/4$ parallel to the imaginary axis, and a Fourier expansion in the angular variable θ to impose periodicity. We plot the function along with the approximation error $|f(x, y) - r(x, y)|$ in Figure 4, and observe a maximum error of 3.6×10^{-13} when evaluating the rational approximant on a 1000×1000 equispaced grid in the radial and angular directions.

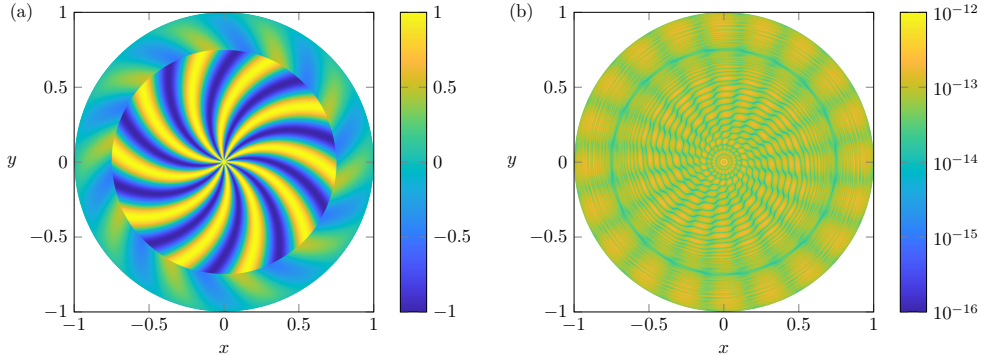


Fig. 4: (a) The function $f(r, \theta)$ defined in (2.10) with discontinuity at $r = 3/4$ and square-root singularity at $r = 1$. (b) The approximation error with the rational approximant, whose poles cluster exponentially fast towards $r = 3/4$ and $r = 1$ from both sides in the imaginary direction.

2.5. Robust and optimal parameter choices. The construction proposed in subsection 2.1 is designed to provide a robust approximation scheme for multivariate functions with edge singularities at known locations. In this section, we first show that the parameter choices described in subsection 2.1 give satisfactory results for a variety of problems. Next, we explain how the approximation scheme can be further optimized when more information on the problem is known.

The influence of the truncation parameter ϵ used in Algorithm 2.1 on the overall convergence behavior and, intrinsically related, on the size of the coefficients can be seen in Figure 5 for the functions f_1 and f_3 introduced in subsection 2.4. The maximum error is again computed on an independent grid consisting of points that are distributed similarly as the sampling points, yet which is much finer than the sampling grid. For branch points singularities, the maximum error on this grid gives a reliable indication of the uniform error on $[0, 1] \times [0, 1]$. For discontinuities, a small error simply indicates high precision up to machine epsilon distance away from the discontinuity. The results for f_2 are analogous to those of f_1 . A comparison is made between $\epsilon = 10^{-14}$ (default, full line) and $\epsilon = 10^{-10}$ (dashed line). Most importantly, Figure 5(a) shows that the approximation achieves high precision even though the system matrices in (2.3) are heavily ill-conditioned. This follows from Theorem 2.1 and the fact that the coefficients of the rational approximants are small at the time of convergence, as can be seen in Figure 5(b). Figure 5(b) also shows that the regularization parameter has an influence on the intermediary growth of the coefficients, a phenomenon which is analyzed in [1, 2]. In this paper a fixed value of $\epsilon = 10^{-14}$ is used, resulting in high accuracy yet suffering from a large intermediary coefficient growth. In [3] it is shown

that this growth can be avoided by varying the regularization parameter with N_q .

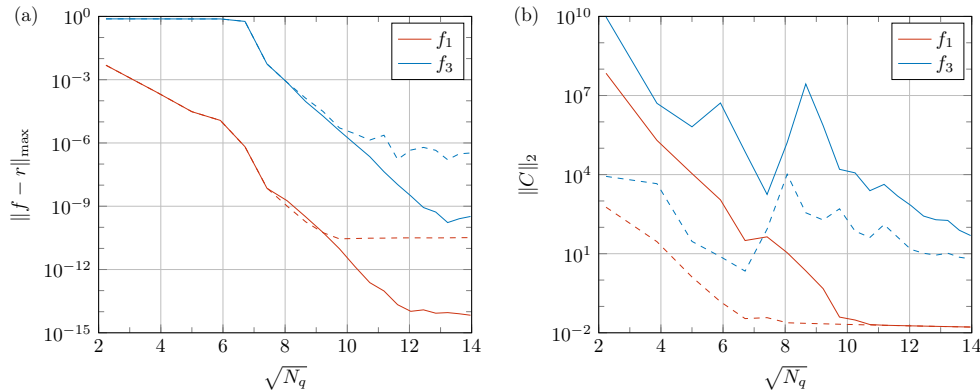


Fig. 5: (a) Approximation error between the rational approximant and the functions $f_1(x, y) = (x(1-x))^{1/4+y}\sqrt{y(1-y)}$ and $f_3(r, \theta)$ defined by (2.10) as a function of $\sqrt{N_q}$, displayed for two values of the truncated SVD parameter in Algorithm 2.1: $\epsilon = 10^{-14}$ (default, full line) and $\epsilon = 10^{-10}$ (dashed line). The figure displays the maximum error on a fine independent grid, similarly distributed as the sampling grid. (b) The Frobenius norm of the coefficient matrix C of the rational approximant to the functions f_1 and f_3 as a function of $\sqrt{N_q}$.

In Figure 6, we illustrate the influence of the parameters σ , which determines the spacing between the clustered poles, and ϵ on the accuracy of a fixed-degree rational approximant to the same functions f_1 , f_2 and f_3 . The default values $\sigma = 2\pi$ and $\epsilon = 10^{-14}$ employed in this paper are marked by a dashed line. It follows from Figure 6(a) that the approximation error shows a clear dependence on σ , materialized by a V-shaped curve for f_1 and f_2 , which is similar to what has been observed in the one-dimensional case [32]. This behavior stems from the balance of the truncation error for small values of σ and the discretization error for large values of σ [32, 48, 53]. The error behaves slightly differently for the discontinuous function f_3 ; the truncation error here drops abruptly once the spacing σ is large enough such that the clustered poles cover the independent sampling grid. Of course the pointwise error always remains $\mathcal{O}(1)$ near the discontinuity itself. Figure 6(b) shows that the approximation error is nearly insensitive to the precise value of ϵ , provided that it is sufficiently small compared to the achievable accuracy, which also followed from Figure 6(a).

Prior research optimized the precise distribution of the preassigned poles in the univariate case when approximating branch point singularities x^α . First, it follows from [53] that a tapered distribution, which we incorporated in (2.1), increases the convergence rate. Furthermore, as can also be seen on Figure 6, optimizing the parameter σ can have a significant effect on the approximation error. [32] shows that the optimal value for σ is a function of the type of the singularity α and the angle (in the complex plane) between the approximation interval and the line on which the poles are clustered. The same dependency is observed for the clustering introduced in the multivariate approximation scheme provided that the dominant singular behavior close to the edge singularity behaves as $\mathcal{O}(d^\alpha)$, where d is the distance to the edge. The most general setting is described in [32, Conj. 5.3], where β relates to the angle. For the multivariate approximation, this angle is defined in a plane perpendicular to the

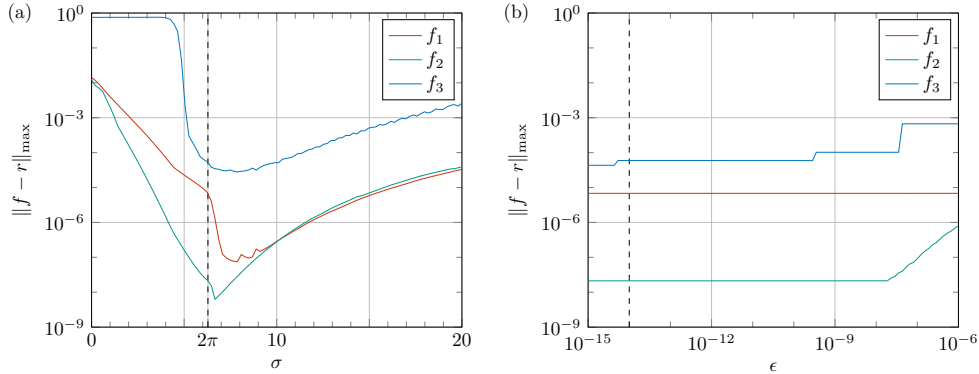


Fig. 6: (a) Evolution of the approximation error with respect to the choice of the parameter σ in (2.1) between the rational approximant and the functions f_1 ($N_q = 40$), f_2 ($N_q = 40$) and f_3 ($N_q = 80$). The vertical dashed line highlights the choice of $\sigma = 2\pi$ employed in this paper. (b) Evolution of the approximation error with respect to the truncated SVD parameter ϵ in Algorithm 2.1. The vertical dashed line highlights the choice of $\epsilon = 10^{-14}$ employed in this paper. The approximation accuracy is insensitive to the choice of ϵ in these examples once ϵ is smaller than the achievable error. Both figures display the maximum error on a fine independent grid, similarly distributed as the sampling grid.

edge singularity. Note that the scheme in subsection 2.1 uses poles that cluster parallel to the positive and negative imaginary axis, corresponding to $\beta = 1$. The parameter setting $\sigma = 2\pi$ used in this paper is therefore chosen such that it is optimal for square root singularities ($\alpha = 1/2$). This can be adapted if the type of the singularity is known. Moreover, if the singularity is located at the boundary of the domain, it is more efficient to use a single set of real poles outside the domain, corresponding to $\beta = 0$. Given more information on the analyticity of the function to be approximated in \mathbb{C}^2 , a single set of imaginary poles might also suffice for singularities located in the interior of the domain. This relates to the principles discussed in [13, section 6].

The numerical scheme is not restricted to the approximation of singularities of type $\mathcal{O}(d^\alpha)$, but can be used to approximate more general *local behavior*, such as discontinuities. To analyze and optimize σ in this general setting, we believe it is beneficial to interpret and view the rational poles as sigmoidal radial basis functions on a logarithmic scale, a concept which was introduced in [35]. As mentioned before, note that the proposed tapered distribution of the poles (2.1) is an optimization linked to the behavior of branch point singularities [35, 53]. For discontinuities, a uniform exponential distribution is observed to be more efficient.

3. Piecewise rational approximation. The multivariate rational approximation algorithm described in section 2 is only valid for product domains of the form $\Omega = I_1 \times I_2$, where $I_1, I_2 \subset \mathbb{R}$ are intervals, and for singularities of the function along straight lines aligning with the boundaries of Ω . However, the scheme extends naturally to polygonal domains and functions with straight line singularities using a domain decomposition technique. One motivation for the approximation of two-dimensional functions with singularities inside the domain arises from the approximation of Green's functions associated with one-dimensional differential operators. For

example, the Green's functions associated with Sturm–Liouville operators on $I \subset \mathbb{R}$ are continuous but not differentiable along the diagonal $\mathcal{D} = \{(x, x), x \in I\}$ of the domain $\Omega = I \times I$ [44, Sec. 15.2.5]. This requires an algorithm for approximating functions with singularities along the diagonal of the domain.

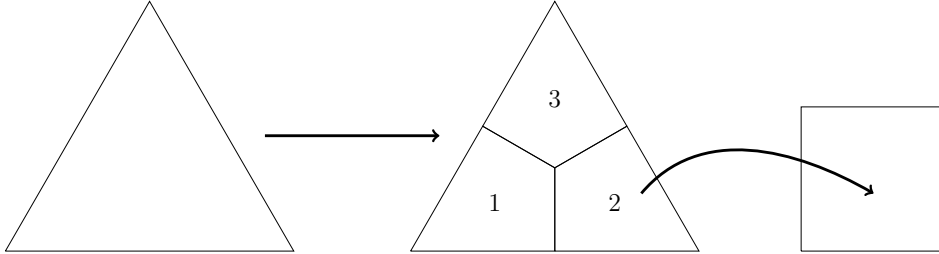


Fig. 7: Diagram illustrating the domain decomposition technique for approximating functions with singularities along straight lines. A decomposition of the domain into triangles is performed by a meshing algorithm. Then, the triangles are refined into three quadrilaterals using a barycentric refinement. Finally, each quadrilateral is mapped into a unit square reference element by an affine transformation.

To approximate a function $f : \Omega \rightarrow \mathbb{R}$ with singularities located along straight lines, we decompose the domain $\Omega \subset \mathbb{R}^2$ into a finite number of subdomains $\Omega = \cup_{i=1}^N \Omega_i$ such that the singularities of the function are located along the boundaries of the subdomains. Here, the subdomains Ω_i are quadrilateral domains with straight line boundaries. This can be achieved using standard meshing software such as Gmsh [27], along with a barycentric refinement of the triangles into quadrilaterals (see Figure 7). Each quadrilateral composing the mesh can then be mapped into a unit square reference element by a rational transformation, for which in our implementation we chose to use the ultraSEM software system [23]. Finally, we approximate the function f independently on each subdomain Ω_i as

$$f(x, y) \approx \sum_{i=1}^N r_i(x, y) \mathbf{1}_{\Omega_i}(x, y), \quad (x, y) \in \Omega,$$

where $\mathbf{1}_{\Omega_i}$ denotes the characteristic function of the domain Ω_i . Here, we perform the rational approximations directly on the reference element using the tensor-product multivariate rational approximation algorithm described in section 2, and map the resulting rational functions back to the domains Ω_i . The transformation to the reference element ensures that the singularities of the function f are located along boundaries of the unit square after the mapping. Hence, one can compute a rational approximation to f on a domain Ω_i using the efficient tensor-product algorithm (see section 2). As long as the number of patches is not too large, the scheme remains efficient overall.

As a numerical example, we consider the piecewise rational approximation of the function f defined on $[0, 1]^2$, with a singularity along the diagonal $x = y$, as

$$(3.1) \quad f(x, y) = \cos(5\pi(x + y)) \sqrt{|x - y|}, \quad (x, y) \in [0, 1]^2.$$

We approximate f using a piecewise rational function consisting of a tensor-product rational function with poles clustering towards the diagonal $x = y$ (see Figure 8).

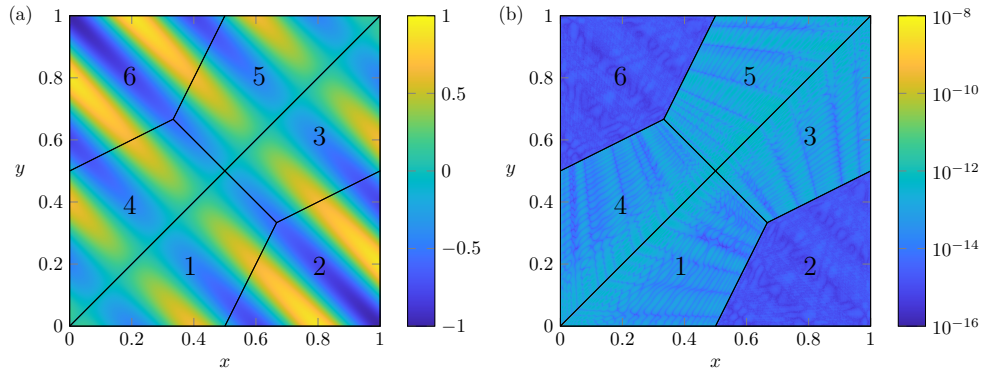


Fig. 8: (a) Piecewise rational approximation to the function f defined on the unit square by (3.1) with singularity located along the diagonal. The domain $\Omega = [0, 1]^2$ is divided into six quadrilaterals so that one can efficiently perform a tensor-product rational approximation of the function on each subdomain. (b) Approximation error between the function f and its piecewise rational approximant on each subdomain of the partition.

We use the method described in subsection 2.1 with rational degree $N_q = 150$ and polynomial degree $N_p = 25$ on the domains $\Omega_1, \Omega_3, \Omega_4, \Omega_5$ (see Figure 8(left)), while we perform a polynomial approximation of degree $N_p = 25$ on Ω_2 and Ω_6 since f is smooth on these domains. We plot the function along with the approximation error $|f(x, y) - r(x, y)|$ in Figure 8 and observe a maximum error of 1.4×10^{-8} when evaluating the rational approximant on a 500×500 equispaced grid on each subdomain.

4. Approximation of functions with curved singularities. Thus far, the constructions in this paper have explored rational approximations in tensor-product form. In the current section we explore more general bivariate rational approximations. Indeed, when the function f has singularities located along curved lines inside the domain Ω , the piecewise rational tensor-product approximation scheme introduced in section 3 is no longer applicable as it would require a very fine refinement of the domain to approximate the singularity curve. Additionally, some applications may require a global rational approximant rather than a piecewise rational expression as in section 3. In this section, we present a method for constructing a multivariate rational approximant to a broad class of functions with singularities along curves. For rational approximations involving such functions we switch from the efficient tensor-product algorithm (Algorithm 2.1) to a direct solver for a large discrete least squares system.

4.1. Methodology. Two general considerations affect the choice of a suitable approximation space. First, the location of the curve influences the denominator of the rational approximations. Here, the question arises how to achieve clustering along curves. Second, the function to be approximated may also exhibit variation along the curve, and this leads to the question of how to represent varying residues in a numerically stable way. We show how to address both of these questions using a number of examples.

We consider functions with singularity located along curves which are precisely the zero-level curves of a polynomial $Q(x, y)$. For example, a diagonal line corresponds to $Q(x, y) = x - y$ and the unit circle to $Q(x, y) = x^2 + y^2 - 1$. We emphasize that this

definition supports multiple singularity curves in the domain through partial fraction representation of $1/Q(x, y)$, such as $Q(x, y) = (x^2 + y^2 - 1)(x^2 + y^2 - (3/4)^2)$ for the function defined in (2.10) and plotted in Figure 4(a), which is singular at the circles of radius $r = 1$ and $r = 3/4$, as well as self-intersecting curves like $Q(x, y) = (x - 1/2)(y - 1/2)$. On the other hand, curves which are not the zero-level of a polynomial would still have to be approximated.

In the most general formulation, we consider a function $f : \Omega = I_1 \times I_2 \subset \mathbb{R}^2 \rightarrow \mathbb{R}$ with polynomial singularity curve located at the roots of a polynomial $Q(x, y)$, and its approximation by a rational function of the form

$$(4.1) \quad r(x, y) = \sum_{j=1}^{N_q} \sum_{0 \leq k, \ell \leq N_p} a_{jkl} \frac{p_j P_k(x) P_\ell(y)}{Q(x, y) - p_j} + \sum_{0 \leq k, \ell \leq N_s} b_{kl} P_k(x) P_\ell(y), \quad (x, y) \in \Omega,$$

where the sequence $\{p_j\}_{j=1}^{N_q}$ clusters exponentially towards zero along the imaginary axis as in (2.1), and the polynomials $\{P_j\}_j$ are chosen to be Chebyshev polynomials (scaled to the intervals I_1 and I_2). The denominators $Q(x, y) - p_j$ may be thought of as clustering curves, in the direction normal to the singularity curve. In the four-dimensional space that arises for complex x and y , these are actually two-dimensional manifolds. The possibility to cluster complex manifolds this way towards a curve in the real plane has been a motivating observation for this paper.

Intuitively, the corresponding residues would vary in the tangential direction, i.e., along the curves. Yet, such behavior is harder to express in general form by means of a polynomial basis for general curves. The form above resorts to a complete bivariate polynomial in tensor-product form in the numerator. One can expect this representation to be highly redundant, but we note that more efficient representations can be found in special cases. We include an example later on.

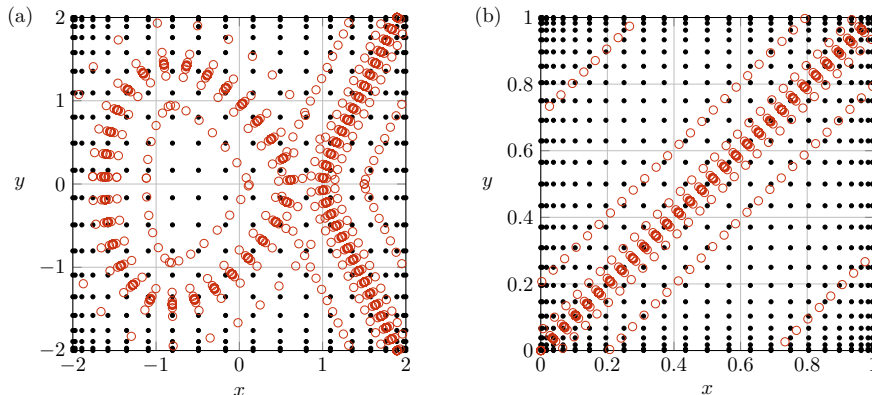


Fig. 9: Sample points used for the numerical examples in subsections 4.2 and 4.3 (a)-(b), which consist of a superposition of a Chebyshev grid (black dots) and points clustering exponentially fast towards the singularity curve in the normal direction (red dots).

We select a set of sample points $\{x_i, y_i\}_{i=1}^M$ as the superposition of Chebyshev points and of points clustering towards the roots of $Q(x, y)$ in the domain Ω , in a

similar manner as section 2. Then, we solve a large least-square system of the form

$$(4.2) \quad \min_{\mathbf{c} \in \mathbb{R}^N} \|\mathbf{A}\mathbf{c} - \mathbf{f}\|_{\mathbb{F}},$$

where the matrix $A \in \mathbb{R}^{N \times M}$ consists of the basis of functions (rationals and polynomials) evaluated at the sample points, $\mathbf{f} = [f(x_1, y_1) \ \dots \ f(x_M, y_M)]^\top$ is the vector of sample values, and $\mathbf{c} \in \mathbb{R}^N$ is a vector containing the $N = N_q(N_p + 1)^2 + (N_s + 1)^2$ coefficients, $\{a_{jkl}\}$ and $\{b_{kl}\}$, of r .

4.2. Singularity along an elliptic curve. In this numerical example, we consider the multivariate rational approximation of the function f on the domain $\Omega = [-2, 2]^2$, defined as

$$f(x, y) = |x^3 - 2x + 1 - y^2|, \quad (x, y) \in [-2, 2]^2.$$

Following the domain of smoothness of the absolute value function, f is continuous everywhere but not differentiable at the points $(x, y) \in [-2, 2]^2$ where f vanishes, *i.e.*, along the elliptic curve defined by the algebraic equation

$$Q(x, y) = x^3 - 2x + 1 - y^2 = 0,$$

whose real graph has two disconnected components since the curve is non-singular [45]. Here, we select the rational, polynomial, and smooth residue degrees in (4.1) as $N_q = 50$, $N_p = 60$, $N_s = 3$, respectively.

Following subsection 4.1, we evaluate the function f at a grid of $M_s \times M_s$ Chebyshev points on $[-2, 2]^2$, where $M_s = 2N_p = 120$. Second, we construct a set of points that cluster towards the singularity curve defined by $Q(x, y) = 0$. To do so, in our implementation we first represent Q by a chebfun2 object in the Chebfun software system [20, 50]. Then, we obtain a complex parameterization of the two disconnected components of the curve as $\gamma_1, \gamma_2 : [-1, 1] \rightarrow \mathbb{C}$ using Chebfun's rootfinding algorithm. This numerical method consists of interpolating the zero level curves of Q by using MATLAB's `contourc` command. For each disconnected component $i \in \{1, 2\}$, we sample the corresponding parameterization γ_i at $M_p = 20$ uniform points $t_1, \dots, t_{M_p} \in [-1, 1]$ to obtain a set of points $\{(\Re(\gamma_i(t_j)), \Im(\gamma_i(t_j)))\}_{j=1}^{M_p}$ located along the disconnected component. For each of these points, we sample f at $M_q = 2N_q$ points clustering exponentially close to the curve in each of the normal directions. We display in Figure 9(a) the sample points used to evaluate the function f and observe the clustering of points colored in red towards the elliptic curve.

Finally, we solve the resulting least-square system (4.2) using MATLAB's backslash command and obtain the coefficients of the rational approximant r to f . We then evaluate the approximation error $|f(x, y) - r(x, y)|$ on a 1000×1000 equispaced grid on $[-2, 2]^2$, and obtain a maximum error of 1.9×10^{-8} . We display in Figure 10 the rational approximant r to f (a) along with the approximation error $|f(x, y) - r(x, y)|$ (b). Moreover, we plot the rational and smooth residue parts of r , corresponding respectively to the two terms in (4.1), in panels (c) and (d).

4.3. Diagonal singularity of a Green's function. As noted in subsection 4.1 a diagonal singularity curve corresponds to $Q(x, y) = x - y$. In this case, variations in the tangential direction can be expressed as a polynomial of $x + y$, since $x + y$ is constant in the normal direction. Thus, we can specialize the general form (4.1) to

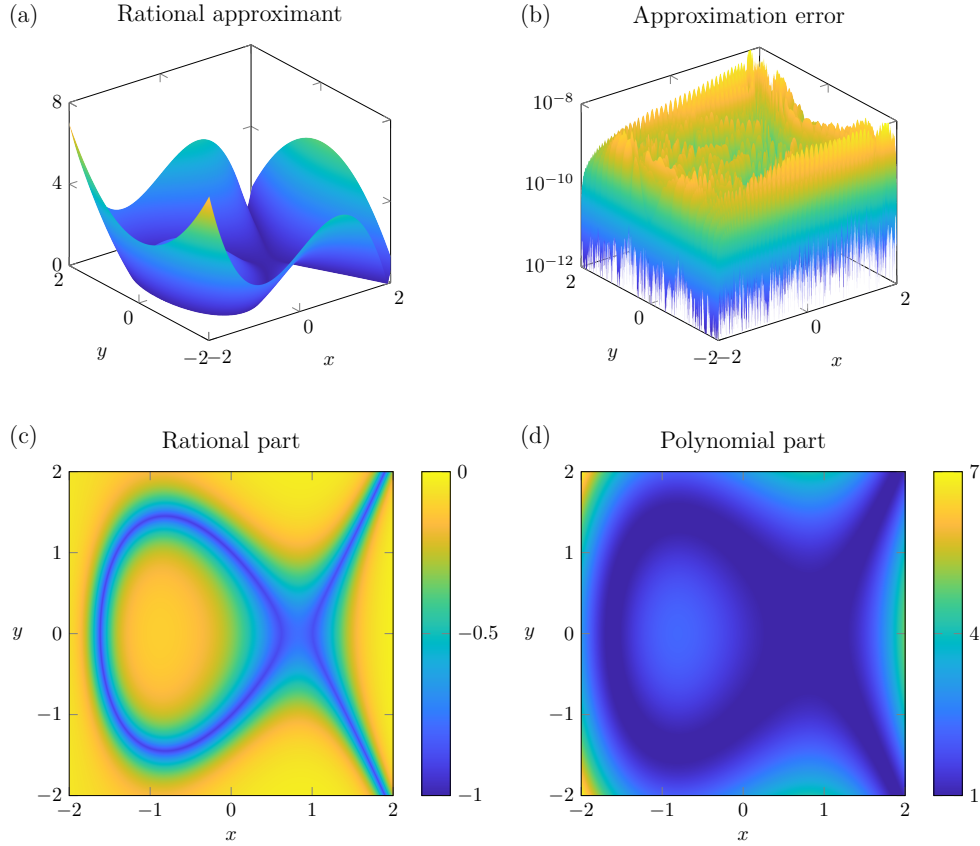


Fig. 10: (a) Multivariate rational approximant $r(x, y)$ to the function $f(x, y) = |x^3 - 2x + 1 - y^2|$, which is not differentiable along an elliptic curve, together with the approximation error $|f(x, y) - r(x, y)|$ (b). (c)-(d) Rational and smooth residue parts of the multivariate approximation.

the more compact representation

$$(4.3) \quad r(x, y) = \sum_{j=1}^{N_q} \sum_{0 \leq k \leq N_p} a_{jk} \frac{p_j P_k(x+y)}{x-y-p_j} + \sum_{0 \leq k, \ell \leq N_s} b_{kl} P_k(x) P_\ell(y), \quad (x, y) \in \Omega.$$

Note the use of a_{jk} in this formula compared to a_{jkl} in (4.1). Unfortunately, it is not the case in general that constant functions in the direction normal to the level-curve of a polynomial are themselves polynomials.

We illustrate the method with a non-trivial example. The Green's function of an elliptic PDE is a bivariate function $G(\mathbf{x}, \mathbf{y})$, which is typically singular along the diagonal $\mathbf{x} = \mathbf{y}$. This function is known analytically for a number of common cases, such as the Laplace and Helmholtz equations, but it has to be computed numerically for differential operators with varying coefficients. In applications such as boundary element methods for integral equations, it is beneficial to have an efficient representation of the Green's function as it has to be evaluated a large number of times.

Here, we construct a multivariate rational approximation to the Green's function

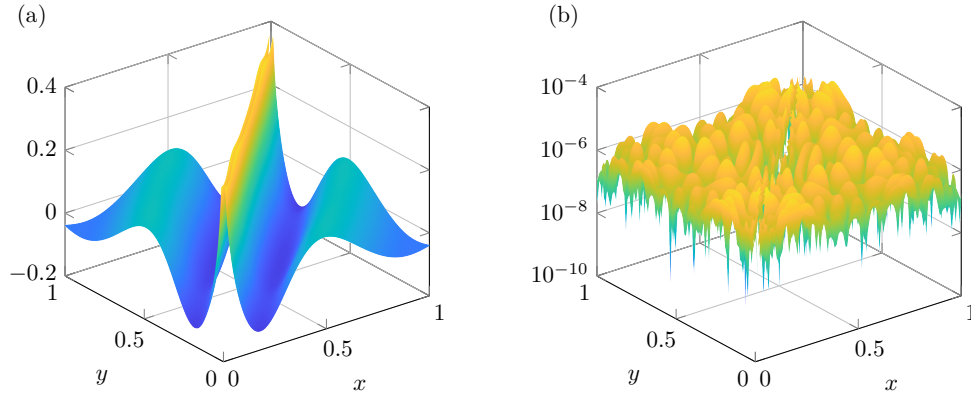


Fig. 11: Approximation of the Green's function $G(\mathbf{x}, \mathbf{y})$ of the gravity Helmholtz equation (as defined in [6]). The function is singular on the diagonal and has wavelike behavior both in the tangential and normal directions. The left panel shows the function for \mathbf{x} and \mathbf{y} varying along a semi-circle, parameterized by $\mathbf{x} = \kappa(x)$ and $\mathbf{y} = \kappa(y)$, leading to a bivariate function on the square $[0, 1]^2$. The right panel shows uniformly high accuracy of the approximation in a dense grid of points, including points close to but excluding the diagonal.

of the so-called *gravity Helmholtz equation* which describes the propagation of waves in a 2D stratified medium [6, 46]. The function has the form [6, (11)]

$$G(\mathbf{x}, \mathbf{y}) = A(\mathbf{x}, \mathbf{y}) \log \frac{1}{|\mathbf{x} - \mathbf{y}|} + B(\mathbf{x}, \mathbf{y}).$$

Mimicking its appearance in a boundary element method, we consider this function with $\mathbf{x}, \mathbf{y} \in \mathbb{R}^2$ varying along the boundary of a domain. Thus, we consider $F(x, y) = G(\kappa(x), \kappa(y))$, in which we have chosen κ as the parameterization of a semi-circle, with so-called energy level $E = 15$ in the definition of the problem. In this experiment we choose $N_q = 25$, $N_p = 5$ and $N_s = 15$, with sampling parameters $M_q = 2N_q$, $M_p = 2N_p$ and $M_s = 2N_s$. Figure 11 illustrates the approximation of the Green's function by the multivariate rational expression along with the approximation error on the domain. Here, we obtain a maximum error of 6×10^{-6} on a 1000×1000 uniform grid.

5. Concluding remarks. In this paper we explored the construction of bivariate rational approximations with fixed, well-chosen poles. When a function has singularities along straight lines, we proposed an efficient tensor-product scheme which converges to nearly machine precision accuracy at a root-exponential rate, as shown by convergence analysis and numerical experiments. The method is based on a least-squares formulation, which can be solved using effective and provably efficient regularization techniques, and generalizes naturally to piecewise rational approximations using domain decompositions. We then presented a global approximation scheme for functions with singularities along curved lines, which is demonstrated on a number of examples, including the approximation of the Green's function associated with the gravity Helmholtz equation, which is singular along the diagonal. An extension to three-dimensional functions is computationally expensive, but straightforward.

Yet, there are several other directions of further research. One open problem is a more efficient solver for the large least squares problems arising in the approximation problems of section 4. A second problem is the compact polynomial representation of tangentially varying residues in that setting. Finally, arguably the largest open challenge is the development of a non-linear adaptive approximation scheme to detect singularities based on function samples, without fixing poles a-priori. Hence, it remains to explore methods that can achieve in multiple dimensions what AAA achieves in the univariate setting.

Code availability. The code needed to reproduce the numerical examples in this paper is available on GitHub at <https://github.com/NBouille/MultivariateRational>.

Acknowledgments. The authors wish to thank Arne Bouillon for the feedback on the manuscript.

Appendix A. Separable truncated SVD algorithm.

An alternative and more straightforward approach to solve the least-square system (2.3) compared to Algorithm 2.1 is to compute the truncated singular value decomposition (SVD) of the matrices A and B separately with a relative truncation parameter ϵ (see Algorithm A.1). This strategy is equivalent to keeping the following singular values of the Kronecker product matrix $B \otimes A$:

$$\{\sigma_k(A)\sigma_\ell(B) \mid \sigma_k(A) \geq \epsilon\sigma_1(A) \text{ and } \sigma_\ell(B) \geq \epsilon\sigma_1(B)\},$$

and preserving some singular values of order $\mathcal{O}(\epsilon^2)$ due to cross-products. However, this leads to a less stable numerical solver for small values of the threshold parameter ϵ , in particular smaller than or close to the square root of machine precision.

Algorithm A.1 Separable truncated SVD solver

Input: $A \in \mathbb{C}^{M_A \times N_A}$, $B \in \mathbb{C}^{M_B \times N_B}$, $F \in \mathbb{C}^{M_A \times M_B}$, relative tolerance $\epsilon > 0$

Output: $C \in \mathbb{C}^{N_A \times N_B}$ such that $ACB^\top \approx F$

- 1: Compute the SVD of A and B , $A = U_A \Sigma_A V_A^*$ and $B = U_B \Sigma_B V_B^*$, where

$$U_A \Sigma_A V_A^* = \begin{bmatrix} U_{A1} & U_{A2} \end{bmatrix} \begin{bmatrix} \Sigma_{A1} & \\ & \Sigma_{A2} \end{bmatrix} \begin{bmatrix} V_{A1} & V_{A2} \end{bmatrix}^*,$$

$$U_B \Sigma_B V_B^* = \begin{bmatrix} U_{B1} & U_{B2} \end{bmatrix} \begin{bmatrix} \Sigma_{B1} & \\ & \Sigma_{B2} \end{bmatrix} \begin{bmatrix} V_{B1} & V_{B2} \end{bmatrix}^*,$$

with $0 \leq \Sigma_{A2} < \epsilon \|A\|_2 I \leq \Sigma_{A1}$ and $0 \leq \Sigma_{B2} < \epsilon \|B\|_2 I \leq \Sigma_{B1}$.

- 2: Return $C = V_{A1} (\Sigma_{A1}^{-1} (U_{A1}^* F U_{B1}^{\top}) \Sigma_{B1}^{-1}) V_{B1}^\top$.
-

Nonetheless, this approach remains theoretically rigorous. Hence, analogously to the bounds introduced in [1, 2, 12], the following theorem shows that the residual of the solution C returned by Algorithm A.1 is of order ϵ for functions f that can be approximated to within ϵ by a tensor-product approximant, i.e., there exists a bounded coefficient matrix $X \in \mathbb{C}^{N_A \times N_B}$, satisfying $\|X\|_F \approx 1$, such that $\|F - AXB^\top\|_F \approx \epsilon$.

THEOREM A.1. *Let $A \in \mathbb{C}^{M_A \times N_A}$, $B \in \mathbb{C}^{M_B \times N_B}$, $F \in \mathbb{C}^{M_A \times M_B}$, and choose a relative threshold parameter of $0 < \epsilon < 1$. Let $C \in \mathbb{C}^{N_A \times N_B}$ be the coefficient matrix computed by Algorithm A.1. Then,*

$$\|F - ACB^\top\|_F \leq \inf_{X \in \mathbb{C}^{N_A \times N_B}} \{2 \|F - AXB^\top\|_F + \gamma_{A,B}^\epsilon \epsilon \|X\|_F\},$$

where $\gamma_{A,B}^\epsilon := (2 + \epsilon) \|A\|_2 \|B\|_2$.

Proof. We substitute

$$C = V_{A_1}(\Sigma_{A_1}^{-1}(U_{A_1}^* F U_{B_1}^{*\top}) \Sigma_{B_1}^{-1}) V_{B_1}^\top = (V_{A_1} \Sigma_{A_1}^{-1} U_{A_1}^*) F (V_{B_1} \Sigma_{B_1}^{-1} U_{B_1}^*)^\top$$

into the residual of (2.3) to obtain

$$\|F - ACB^\top\|_F = F - A(V_{A_1} \Sigma_{A_1}^{-1} U_{A_1}^*) F (V_{B_1} \Sigma_{B_1}^{-1} U_{B_1}^*)^\top B^\top.$$

One can expand the block form of the SVD of A into $A = U_{A_1} \Sigma_{A_1} V_{A_1}^* + U_{A_2} \Sigma_{A_2} V_{A_2}^*$ and B into $B = U_{B_1} \Sigma_{B_1} V_{B_1}^* + U_{B_2} \Sigma_{B_2} V_{B_2}^*$, with $V_{A_1}^* V_{A_2}^* = 0$ and $V_{B_1}^* V_{B_2}^* = 0$. Therefore,

$$\begin{aligned} AV_{A_1} \Sigma_{A_1}^{-1} U_{A_1}^* &= U_{A_1} \Sigma_{A_1} V_{A_1}^* V_{A_1} \Sigma_{A_1}^{-1} U_{A_1}^* + U_{A_2} \Sigma_{A_2} V_{A_2}^* V_{A_1} \Sigma_{A_1}^{-1} U_{A_1}^* \\ &= U_{A_1} \Sigma_{A_1} \Sigma_{A_1}^{-1} U_{A_1}^* = U_{A_1} U_{A_1}^* \end{aligned}$$

and similarly

$$(V_{B_1} \Sigma_{B_1}^{-1} U_{B_1}^*)^\top B^\top = (B V_{B_1} \Sigma_{B_1}^{-1} U_{B_1}^*)^\top = (U_{B_1} U_{B_1}^*)^\top.$$

For any $X \in \mathbb{C}^{N_A \times N_B}$, we can add and subtract $AXB^\top - U_{A_1} U_{A_1}^* (AXB^\top) (U_{B_1} U_{B_1}^*)^\top$ to get

$$\begin{aligned} F - ACB^\top &= \underbrace{(F - AXB^\top) - U_{A_1} U_{A_1}^* (F - AXB^\top) (U_{B_1} U_{B_1}^*)^\top}_1 \\ &\quad + \underbrace{AXB^\top - U_{A_1} U_{A_1}^* (AXB^\top) (U_{B_1} U_{B_1}^*)^\top}_2. \end{aligned}$$

Using the standard inequalities $\|AB\|_F \leq \|A\|_2 \|B\|_F$ and $\|AB\|_F \leq \|A\|_F \|B\|_2$ [33, §50.3], the Frobenius norm of the first term can be bounded by

$$\begin{aligned} &\|(F - AXB^\top) - U_{A_1} U_{A_1}^* (F - AXB^\top) (U_{B_1} U_{B_1}^*)^\top\|_F \\ &\leq (1 + \|U_{A_1} U_{A_1}^*\|_2 \|(U_{B_1} U_{B_1}^*)^\top\|_2) \|F - AXB^\top\|_F \\ &\leq 2 \|F - AXB^\top\|_F. \end{aligned}$$

Again using the expansion of the block form of the SVD, the second term can be written as

$$\begin{aligned} &AXB^\top - U_{A_1} U_{A_1}^* (AXB^\top) (U_{B_1} U_{B_1}^*)^\top \\ &= (U_{A_1} \Sigma_{A_1} V_{A_1}^* + U_{A_2} \Sigma_{A_2} V_{A_2}^*) X (U_{B_1} \Sigma_{B_1} V_{B_1}^* + U_{B_2} \Sigma_{B_2} V_{B_2}^*)^\top \\ &\quad - (U_{A_1} \Sigma_{A_1} V_{A_1}^*) X (U_{B_1} \Sigma_{B_1} V_{B_1}^*)^\top \\ &= (U_{A_1} \Sigma_{A_1} V_{A_1}^*) X (U_{B_2} \Sigma_{B_2} V_{B_2}^*)^\top + (U_{A_2} \Sigma_{A_2} V_{A_2}^*) X (U_{B_1} \Sigma_{B_1} V_{B_1}^*)^\top \\ &\quad + (U_{A_2} \Sigma_{A_2} V_{A_2}^*) X (U_{B_2} \Sigma_{B_2} V_{B_2}^*)^\top. \end{aligned}$$

Therefore,

$$\begin{aligned} &\|AXB^\top - U_{A_1} U_{A_1}^* (AXB^\top) (U_{B_1} U_{B_1}^*)^\top\|_F \\ &\leq (\|\Sigma_{A_1}\|_2 \|\Sigma_{B_2}\|_2 + \|\Sigma_{A_2}\|_2 \|\Sigma_{B_1}\|_2 + \|\Sigma_{A_2}\|_2 \|\Sigma_{B_2}\|_2) \|X\|_F. \end{aligned}$$

The final bound follows from

$$\|\Sigma_{A_1}\|_2 \leq \|A\|_2, \quad \|\Sigma_{A_2}\|_2 \leq \epsilon \|A\|_2, \quad \|\Sigma_{B_1}\|_F \leq \|B\|_2, \quad \|\Sigma_{B_2}\|_F \leq \epsilon \|B\|_2. \quad \square$$

Remark A.2. Algorithm A.1 and the statement of Theorem A.1, as well as its proof, can also be formulated for 3D or higher-dimensional approximations with only minor changes. The rationale is that the regularization is applied in each dimension independently.

Appendix B. Convergence of the univariate lightning approximation.

The following two lemmas correspond to Theorem 2.2 and Theorem 2.3 of [29], respectively. The first lemma is a local statement about approximation near a singularity, while the second lemma describes approximation on the interval $[0, 1]$. The results were not explicitly stated in [29] as we formulate them here, hence we include short proofs. The first lemma specifies an a priori choice of poles in the unit disk $D(0, 1)$ on the interval $[-1, 0]$.

LEMMA B.1. *Let f satisfy the conditions of [29, Thm. 2.2], and define all symbols as in that theorem, in particular the poles $p_j = e^{-\sigma j/\sqrt{n}}$ for some $\sigma > 0$ and $0 \leq j \leq n - 1$. Assume in addition that $|f(z)| \leq D|z|^\delta$ with $D > 0$ and z in a disk with radius b around the origin. There exists an $n_0 > 0$ sufficiently large, depending on $b > 0$ but not on f , and a type $(n - 1, n)$ rational function r_n such that for $z \in [0, \rho]$*

$$|f(z) - r_n(z)| \leq A_0 D \|f\|_{\infty, D(0,1)} e^{-C\sqrt{n}}, \quad n > n_0,$$

where A_0 is independent of f . Here, the constant C depends only on δ and on σ , while ρ is sufficiently small and satisfies $0 < \rho < 1$ and depends only on σ .

Proof. The proof of [29, Thm. 2.2] shows that constants A and C exist such that

$$|f(z) - r(z)| \leq A e^{-C\sqrt{n}}, \quad n \geq 1,$$

for z in a wedge centered at $z = 0$ with angle θ and radius $0 < \rho < 1$. For the constant C , we merely note that it is determined by the distribution of poles and by the value of δ . The value of ρ depends only on the distribution of poles, i.e., on σ . We can arbitrarily choose the angle θ of the wedge, as we are only interested in its intersection $[0, \rho]$ with the real line.

The constant A is more involved. In the cited proof, it arises from two applications of a Hölder inequality, giving rise to $A = A_1 + A_2$. The first application uses $|f(z)| = \mathcal{O}(|z|^\delta)$ on the interval $[-\epsilon, 0]$, in which $-\epsilon = -e^{-\sigma(n-1)/\sqrt{n}}$ is the smallest pole. We take n_0 sufficiently large so that we may use the bound $|f(z)| \leq D|z|^\delta$ instead, showing that A_1 is proportional to D but independent of f .

The second application leads to A_2 being proportional to $\max_{z \in [0, \rho]} \int_{\Gamma_1} \left| \frac{f(t)}{t-z} \right| dt$, in which Γ_1 is the unit circle with -1 connected to $-\epsilon$ both above and below the slit [29, Fig. 2]. The integrand can be bounded by substituting f with $\|f\|_{\infty, D(0,1)}$, if $|t| > b$, and by $D|t|^\delta$, if $|t| \leq b$. This leads to a bound that is proportional to these constants. Note that the different bound in the disk of radius b is necessary for the Cauchy integral to be bounded uniformly in n , since the integral is finite as $-\epsilon$ approaches zero from the left and z approaches zero from the right only because f vanishes at the origin. \square

The second lemma involves a scaling with a factor $R > 1$, which in principle maps those poles to a larger interval $[-R, 0]$. However, both in theory and in practice, the poles can be scaled essentially to an arbitrary interval near the singularity. On the one hand, what matters is not the precise formula for the poles but their density close to the singularity. On the other hand, rational functions with poles further away can always be absorbed into the polynomial part, hence the scaling is not critical. The

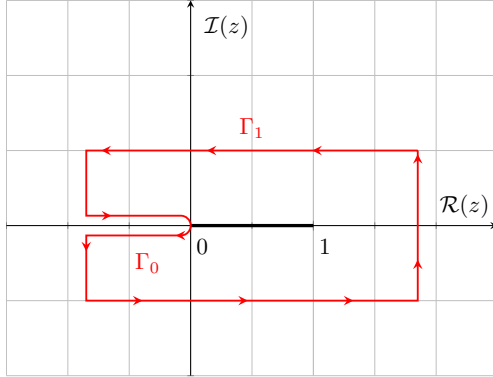


Fig. 12: The approximation problem of Lemma B.2. The contour $\Gamma = \Gamma_0 \cup \Gamma_1$ lies in the closure of the region of analyticity of f .

rate of convergence C is more sensitive to the choice of σ , which governs the density of small poles, than it is to other parameters, but convergence is root-exponential no matter how σ and the scaling of the poles are chosen.

LEMMA B.2. *Let f be analytic on a complex neighborhood Ω of $[0, 1]$, but excluding a slit along the negative real axis up to and including the point $z = 0$. Assume that f satisfies $|f(z)| \leq D|z|^\delta$ for some $\delta > 0$ and z in a disk of radius $b > 0$ around the origin. Then, there exist type $(n + m, n)$ rational approximations $r_{n+m, n}$ and a constant $C > 0$, independent of f , such that*

$$\|f - r_{n+m, n}\|_{\infty, [0, 1]} \leq AD \|f\|_{\infty, \Omega} e^{-C\sqrt{n}}, \quad n > n_0,$$

for some sufficiently large $n_0 > 0$. Moreover, the polynomial part can be chosen to have degree $m = E\sqrt{n}$, for a sufficiently large constant $E > 0$ that also scales with $\|f\|_{\infty, \Omega}$, and the rational functions can be chosen to have simple poles at

$$(B.1) \quad \beta_j = -R e^{-\sigma j / \sqrt{n}}, \quad 0 \leq j \leq n - 1,$$

with $\sigma > 0$ and for some sufficiently large $R > 1$ independent of f . The constant A depends on the region of analyticity Ω and on the radius b , but is independent of f and of n .

Proof. Root-exponential convergence of rational approximations of the required form is proven in [29, Thm. 2.3] for f analytic on a polygonal region $\Omega \subset \mathbb{C}$, with slits along the exterior bisector at corners. The current statement differs from the stated result in two ways: (i) we take Ω to be $[0, 1]$ and we consider possible lack of analyticity only at the left endpoint $z = 0$, and (ii) we make the dependence on f more explicit. The method of proof is entirely the same as that of [29, Theorem 2.3] and here we focus mainly on these two differences.

For the region, we substitute the contour Γ and its constituent parts of [29, Thm. 2.3] by those shown in Figure 12. Thus, Γ_0 is a contour from $z = -\eta$ to $z = 0$ and back along both sides of the slit and the contour Γ_1 encircles $[0, 1]$ with positive orientation, while both η and the distance of Γ_1 to the real line are small enough for Γ to remain within the region of analyticity Ω of f . We can write $f = f_0 + f_1$ with

$$f_0 = \frac{1}{2\pi i} \int_{\Gamma_0} \frac{f(t)}{t - z} dt \quad \text{and} \quad f_1 = \frac{1}{2\pi i} \int_{\Gamma_1} \frac{f(t)}{t - z} dt.$$

As in the proof of [29, Thm. 2.3], the function f_1 is analytic away from Γ_1 in some open region containing $[0, 1]$. Hence it can be approximated with exponential convergence by polynomials, with a bound satisfying [52, Thm. 8.2]

$$\|f_1 - p_m\|_{\infty, [0,1]} \leq \frac{2M\xi^{-m}}{\xi - 1},$$

with $\xi > 0$ independent of f and with M the maximum of f_1 along the Bernstein ellipse with radius ξ (within the region of analyticity of f_1). This results in root-exponential convergence in n of this “smooth part” of the problem when the polynomial degree is chosen to be $m = E\sqrt{n}$ for some $E > 0$. The factor in front depends on M , which can readily be bounded in terms of the maximum of f in Ω .

The function f_0 is analytic away from Γ_0 , but may be singular at the endpoint $z = -\eta$ of the contour. For this function, in the proof of [29, Thm. 2.3] the local result [29, Thm. 2.2] is invoked with a scaling factor $1/\rho$ which ensures that the result of that theorem on the interval $[0, \rho]$ implies the approximation of f_0 on $[0, 1]$. The analogue in the current proof is to invoke the local result of Lemma B.1 instead. However, the singularity at $z = -\eta$ is a problem for the factor $\|f\|_{\infty, D(0,1)}$ in the error bound. Hence, we scale by $R > 1/\min(\eta, \rho)$ instead, ensuring that the result of Lemma B.1 implies approximation accuracy on an interval at least as large as $[0, 1]$, while $\tilde{f}_0(z) = f_0(Rz)$ is bounded on the unit disk. Furthermore, as in the proof of [29, Thm. 2.3], $\tilde{f}_0(z) = \mathcal{O}(|z|^\delta)$ as $z \rightarrow 0$ can always be ensured by subtracting a constant from \tilde{f}_0 , to be absorbed in the polynomial term. Though the bound $|\tilde{f}_0| \leq D|z|^\delta$ in Lemma B.1 may involve different constants from those of f with the same name in the current theorem, and in particular the radius in which the bound hold may be a factor R smaller, the precise relationship between the constants is fixed and independent of f , and the bound itself scales linearly with D of the current theorem. Finally, we note that $\|\tilde{f}_0\|_{\infty, D(0,1)}$ can be bounded in terms of $\|f\|_{\infty, \Omega}$. \square

REFERENCES

- [1] B. ADCOCK AND D. HUYBRECHS, *Frames and numerical approximation*, SIAM Rev., 61 (2019), pp. 443–473.
- [2] B. ADCOCK AND D. HUYBRECHS, *Frames and numerical approximation II: Generalized sampling*, J. Fourier Anal. Appl., 26 (2020), pp. 1–34.
- [3] B. ADCOCK AND M. SEIFI, *Frame approximation with bounded coefficients*, Adv. Comput. Math., 47 (2021), pp. 1–25.
- [4] A. P. AUSTIN, M. KRISHNAMOORTHY, S. LEYFFER, S. MRENNNA, J. MÜLLER, AND H. SCHULZ, *Practical algorithms for multivariate rational approximation*, Comput. Phys. Commun., 261 (2021), p. 107663.
- [5] P. J. BADDOO, *Lightning solvers for potential flows*, Fluids, 5 (2020), p. 227.
- [6] A. H. BARNETT, B. J. NELSON, AND J. M. MAHONEY, *High-order boundary integral equation solution of high frequency wave scattering from obstacles in an unbounded linearly stratified medium*, J. Comput. Phys., 297 (2015), pp. 407–426.
- [7] J.-P. BERRUT AND G. ELEFANTE, *A linear barycentric rational interpolant on starlike domains*, arXiv preprint arXiv:2104.09246, (2021).
- [8] N. BOULLÉ, C. J. EARLS, AND A. TOWNSEND, *Data-driven discovery of Green’s functions with human-understandable deep learning*, Sci. Rep., 12 (2022), p. 4824.
- [9] N. BOULLÉ, Y. NAKATSUKASA, AND A. TOWNSEND, *Rational neural networks*, in Advances in Neural Information Processing Systems, vol. 33, 2020, pp. 14243–14253.
- [10] P. D. BRUBECK AND L. N. TREFETHEN, *Lightning stokes solver*, SIAM J. Sci. Comput., 44 (2022), pp. A1205–A1226.
- [11] E. J. CANDÈS AND D. L. DONOHO, *New tight frames of curvelets and optimal representations of objects with c^2 singularities*, Comm. Pure Appl. Math., 57 (2002), pp. 219–266.

- [12] V. COPPÉ, D. HUYBRECHS, R. MATTHYSEN, AND M. WEBB, *The AZ algorithm for least squares systems with a known incomplete generalized inverse*, SIAM J. Matrix Anal. Appl., 41 (2020), pp. 1237–1259.
- [13] S. COSTA AND L. N. TREFETHEN, *AAA-least squares rational approximation and solution of Laplace problems*, arXiv preprint arXiv:2107.01574, (2021).
- [14] A. CUYT AND X. YANG, *A practical error formula for multivariate rational interpolation and approximation*, Numer. Alg., 55 (2010), pp. 233–243.
- [15] A. A. M. CUYT, *Multivariate Padé-approximants*, J. Math. Anal. Appl., 96 (1983), pp. 283–293.
- [16] A. A. M. CUYT AND B. M. VERDONK, *Multivariate rational interpolation*, Computing, 34 (1985), pp. 41–61.
- [17] R. A. DEVORE, *Maximal functions and their application to rational approximation*, in CBMS Regional Conf. Ser. Math., vol. 3, Amer. Math. Soc., 1983, pp. 143–155.
- [18] R. A. DEVORE AND X.-M. YU, *Multivariate rational approximation*, Trans. Amer. Math. Soc., 293 (1986), pp. 161–169.
- [19] T. DRISCOLL, Y. NAKATSUKASA, AND L. N. TREFETHEN, *AAA rational approximation on a continuum*, arXiv preprint arXiv:2305.03677, (2023).
- [20] T. A. DRISCOLL, N. HALE, AND L. N. TREFETHEN, *Chebfun guide*, 2014.
- [21] H. W. ENGL, M. HANKE, AND A. NEUBAUER, *Regularization of inverse problems*, vol. 375, Springer Science & Business Media, 1996.
- [22] L. C. EVANS, *Partial differential equations*, American Mathematical Society, 2nd ed., 2010.
- [23] D. FORTUNATO, N. HALE, AND A. TOWNSEND, *The ultraspherical spectral element method*, J. Comput. Phys., 436 (2021), p. 110087.
- [24] E. S. GAWLIK, *Zolotarev iterations for the matrix square root*, SIAM J. Matrix Anal. Appl., 40 (2019), pp. 696–719.
- [25] E. S. GAWLIK AND Y. NAKATSUKASA, *Zolotarev’s fifth and sixth problems*, arXiv preprint arXiv:2011.10877, (2020).
- [26] E. S. GAWLIK AND Y. NAKATSUKASA, *Approximating the p th root by composite rational functions*, J. Approx. Theory, 266 (2021), p. 105577.
- [27] C. GEUZAINÉ AND J.-F. REMACLE, *Gmsh: A 3-D finite element mesh generator with built-in pre-and post-processing facilities*, Int. J. Numer. Methods Eng., 79 (2009), pp. 1309–1331.
- [28] A. GOPAL AND L. N. TREFETHEN, *New Laplace and Helmholtz solvers*, Proc. Natl. Acad. Sci. U.S.A., 116 (2019), pp. 10223–10225.
- [29] A. GOPAL AND L. N. TREFETHEN, *Solving Laplace problems with corner singularities via rational functions*, SIAM J. Numer. Anal., 57 (2019), pp. 2074–2094.
- [30] N. HALKO, P.-G. MARTINSSON, AND J. A. TROPP, *Finding structure with randomness: Probabilistic algorithms for constructing approximate matrix decompositions*, SIAM Rev., 53 (2011), pp. 217–288.
- [31] P. C. HANSEN, V. PEREYRA, AND G. SCHERER, *Least squares data fitting with applications*, JHU Press, 2013.
- [32] A. HERREMANS, D. HUYBRECHS, AND L. N. TREFETHEN, *Resolution of Singularities by Rational Functions*, SIAM J. Numer. Anal., 61 (2023), pp. 2580–2600.
- [33] L. HOGBEN, *Handbook of linear algebra*, CRC press, 2006.
- [34] D. HUYBRECHS AND L. N. TREFETHEN, *AAA interpolation of equispaced data*, BIT Numer. Math., 63 (2023), p. 21.
- [35] D. HUYBRECHS AND L. N. TREFETHEN, *Sigmoid functions and multiscale resolution of singularities*, arXiv preprint arXiv:2303.01967, (2023).
- [36] G. E. KARNIADAKIS, I. G. KEVREKIDIS, L. LU, P. PERDIKARIS, S. WANG, AND L. YANG, *Physics-informed machine learning*, Nat. Rev. Phys., 3 (2021), pp. 422–440.
- [37] Z. MAO, A. D. JAGTAP, AND G. E. KARNIADAKIS, *Physics-informed neural networks for high-speed flows*, Comput. Methods Appl. Mech. Eng., 360 (2020), p. 112789.
- [38] C. MARCATI, J. A. OPSCHOOR, P. C. PETERSEN, AND C. SCHWAB, *Exponential ReLU neural network approximation rates for point and edge singularities*, Found. Comput. Math., 23 (2023), pp. 1043–1127.
- [39] P.-G. MARTINSSON AND J. A. TROPP, *Randomized numerical linear algebra: Foundations and algorithms*, Acta Numer., 29 (2020), pp. 403–572.
- [40] Y. NAKATSUKASA, O. SÈTE, AND L. N. TREFETHEN, *The AAA algorithm for rational approximation*, SIAM J. Sci. Comput., 40 (2018), pp. A1494–A1522.
- [41] Y. NAKATSUKASA AND L. N. TREFETHEN, *An algorithm for real and complex rational minimax approximation*, SIAM J. Sci. Comput., 42 (2020), pp. A3157–A3179.
- [42] A. NEUMAIER, *Solving ill-conditioned and singular linear systems: A tutorial on regularization*, SIAM Rev., 40 (1998), pp. 636–666.
- [43] D. J. NEWMAN, *Rational approximation to $|x|$* , Mich. Math. J., 11 (1964), pp. 11–14.

- [44] K. F. RILEY, M. P. HOBSON, AND S. J. BENICE, *Mathematical methods for physics and engineering*, Cambridge University Press, 3rd ed., 2006.
- [45] J. H. SILVERMAN, *The arithmetic of elliptic curves*, Springer, 2009.
- [46] R. M. SLEVINSKY AND S. OLVER, *A fast and well-conditioned spectral method for singular integral equations*, *J. Comput. Phys.*, 332 (2017), pp. 290–315.
- [47] H. STAHL, *Best uniform rational approximation of x^α on $[0, 1]$* , *Bull. Am. Math. Soc.*, 28 (1993), pp. 116–122.
- [48] H. STAHL, *Poles and zeros of best rational approximants of $|x|$* , *Constr. Approx.*, 10 (1994), pp. 469–522.
- [49] E. STEPHAN AND J. WHITEMAN, *Singularities of the Laplacian at corners and edges of three-dimensional domains and their treatment with finite element methods*, *Math. Methods Appl. Sci.*, 10 (1988), pp. 339–350.
- [50] A. TOWNSEND AND L. N. TREFETHEN, *An extension of Chebfun to two dimensions*, *SIAM J. Sci. Comput.*, 35 (2013), pp. C495–C518.
- [51] L. TREFETHEN, *Multivariate polynomial approximation in the hypercube*, *Proc. Amer. Math. Soc.*, 145 (2017), pp. 4837–4844.
- [52] L. N. TREFETHEN, *Approximation Theory and Approximation Practice*, SIAM, Philadelphia, extended ed., 2019.
- [53] L. N. TREFETHEN, Y. NAKATSUKASA, AND J. WEIDEMAN, *Exponential node clustering at singularities for rational approximation, quadrature, and PDEs*, *Numer. Math.*, 147 (2021), pp. 227–254.
- [54] L. N. TREFETHEN, Y. NAKATSUKASA, AND J. A. C. WEIDEMAN, *Exponential node clustering at singularities for rational approximation, quadrature, and PDEs*, *Numer. Math.*, 147 (2021), pp. 227–254.
- [55] C. F. VAN LOAN AND N. PITSIANIS, *Approximation with Kronecker products*, in *Linear Algebra for Large Scale and Real-Time Applications*, Springer, 1993, pp. 293–314.
- [56] Y. XUE, S. L. WATERS, AND L. N. TREFETHEN, *Computation of 2D Stokes flows via lightning and AAA rational approximation*, arXiv preprint arXiv:2306.13545, (2023).
- [57] S. YANG AND S. XIANG, *Fast barycentric rational interpolations for complex functions with some singularities*, *Calcolo*, 60 (2023), p. 55.
- [58] E. ZOLOTAREV, *Application of elliptic functions to questions of functions deviating least and most from zero*, *Zap. Imp. Akad. Nauk. St. Petersburg*, 30 (1877), pp. 1–59.